6-8-2020

Characterization of Ice Adhesion: Approaches and Modes of Loading

Bishoy Dawood
Iowa State University, bdawood@iastate.edu

Denizhafn Yavas
Iowa State University

Christopher J. Giuffre
Iowa State University, cgiuffre@iastate.edu

Ashraf Bastawros
Iowa State University, bastaw@iastate.edu

Characterization of Ice Adhesion: Approaches and Modes of Loading

Abstract

Airborne structures are vulnerable to atmospheric icing in cold weather operation conditions. Most of the ice adhesion-related works have focused on mechanical ice removal strategies because of practical considerations, while limited literature is available for a fundamental understanding of the ice adhesion process. Here, we present fracture mechanics-based approaches to characterize interfacial fracture parameters for the tensile and shear behavior of a typical ice/aluminum interface. An experimental framework employing single cantilever beam, direct shear, and push-out shear tests were developed to achieve near mode-I and near mode-II fracture conditions at the interface. Both analytical (beam bending and shear-lag analysis), and numerical (finite element analysis incorporating cohesive zone method) models were used to extract mode-I and II interfacial fracture parameters. The combined experimental and numerical results, as well as surveying published results for the direct shear and push-out shear tests, showed that mode-II interfacial strength and toughness could be significantly affected by the test method due to geometrically induced interfacial residual stress. As a result, the apparent toughness of the zero-angle push-out test could reach an order of magnitude higher than those derived from direct shear tests. Moreover, it was found that the interfacial ice adhesion is fracture mode insensitive and roughness insensitive for tensile and shear modes, for the observed modes of failures in this study

Disciplines

Aeronautical Vehicles | Structures and Materials

Comments

This is a manuscript of a proceeding published as Dawood, B., Yavas, D., Giuffre, C.J. and Bastawros, A. "Characterization of Ice Adhesion: Approaches and Modes of Loading." Paper No. AIAA 2020-2802. In *AIAA AVIATION 2020 Forum*. (2020): 2802. DOI: 10.2514/6.2020-2802. Posted with permission.

AIAA Paper No. AIAA 2020-2802
AIAA AVIATION 2020 Forum, June 15-19, 2020, VIRTUAL EVENT
https://doi.org/10.2514/6.2020-2802

Characterization of Ice Adhesion: Approaches and Modes of Loading

Bishoy Dawood[1], Denizhafn Yavas[2] and Ashraf F. Bastawros[3]
Department of Aerospace Engineering, Iowa State University, Ames. IA, 50011, USA

Airborne structures are vulnerable to atmospheric icing in cold weather operation conditions. Most of the ice adhesion-related works have focused on mechanical ice removal strategies because of practical considerations, while limited literature is available for a fundamental understanding of the ice adhesion process. Here, we present fracture mechanics-based approaches to characterize interfacial fracture parameters for the tensile and shear behavior of a typical ice/aluminum interface. An experimental framework employing single cantilever beam, direct shear, and push-out shear tests were developed to achieve near mode-I and near mode-II fracture conditions at the interface. Both analytical (beam bending and shear-lag analysis), and numerical (finite element analysis incorporating cohesive zone method) models were used to extract mode-I and II interfacial fracture parameters. The combined experimental and numerical results, as well as surveying published results for the direct shear and push-out shear tests, showed that mode-II interfacial strength and toughness could be significantly affected by the test method due to geometrically induced interfacial residual stress. As a result, the apparent toughness of the zero-angle push-out test could reach an order of magnitude higher than those derived from direct shear tests. Moreover, it was found that the interfacial ice adhesion is fracture mode insensitive and roughness insensitive for tensile and shear modes, for the observed modes of failures in this study.

I. Nomenclature

a	=	Crack length
a_o	=	Initial crack length
b	=	Ice length along loading
B	=	Ice width
CZM	=	Cohesive zone method
E	=	Young's modulus
G	=	Energy release rate
h	=	Ice height or thickness
K	=	Initial stiffness for the traction-separation law
P	=	Applied load
RMS	=	Root mean square surface roughness
SCB	=	Single cantilever beam
δ	=	Displacement
Γ_I	=	Interfacial fracture toughness in mode I
Γ_{II}	=	Interfacial fracture toughness in mode II
τ_c	=	Interfacial shear strength

[1] Graduate Student, Department of Aerospace Engineering, Iowa State University.
[2] Postdoctoral Fellow, Department of Aerospace Engineering, Iowa State University.
[3] T.A. Wilson Professor of Engineering, Department of Aerospace Engineering, Iowa State University.

II. Introduction

Ice accretion is a natural hazard that impacts the performance of different engineering structures, including land [1], sea [2], and airborne transportation systems [3, 4], and energy infrastructure for power transmission lines [5] and wind turbine energy harnessing systems [6]. The performance, as well as the safety of these structures, can be significantly degraded due to the ice accretion on its control surfaces [7, 8]. Icing on aircrafts results in increased drag with possible interference with lift forces and potential catastrophic events. While anti-icing surfaces and de-icing mechanisms play a crucial role on the performance of these systems, understanding of the ice removal mechanism is crucial to design and optimize the force and energy requirements for different ice protection systems to ensure shedding of accreted ice. The ice adhesion strength at the ice-solid interface is one of the critical parameters to gage the surface icephobic ability. The ice adhesion strength has been studied over the past 70 years through different types of mechanical testing configurations, including push-out, direct shear, cylindrical twist of normal interface, and centrifuge configuration [8-16]. The differences in experimental measurement techniques can be grouped into two major categories based on the application of the peel-off force; (a) centrifuge and vibration tests [17-18] to shear off the interface via centripetal forces or vibrational amplitude, and (b) direct mechanical tests such as 0° cone test (similar to the push-out configuration), and direct shear configuration [11, 19-20]. In addition, water contact angle measurements have been widely used to estimate ice adhesion and have shown a good correlation between water wettability and adhesion strength [21]. With diverse testing configurations and experimental testing environment, a wide range of ice adhesion shear strength on typical metallic surfaces was reported with more than an order of magnitude of variance of 70-2,500 kPa [15], as summarized on Fig. 1, for a typical ice-aluminum interface. One of the key differences can be attributed to the difference between the push-out test and those of direct shear, and centrifuge tests. For example, the shear strength of a typical ice/aluminum interface was measured to be 100-300 kPa by the direct shear testing configuration [22], whereas shear strength was found significantly higher of about 1000-3000 kPa, using 0˚cone test for a similar interface under similar test temperature and conditions [11, 22-23]. These tests are considered a strength-based measurement where the bonding strength of ice/substrate was characterized by measuring the interfacial shear strength, and very little work has utilized the fracture mechanics approach to accurately understand the mechanics of ice shedding [24, 25]. Such limit load interpretation of the ice-solid interface ignores the role of micro-structural and interfacial defects, as well as the geometrical constraints arising from different testing methodologies.

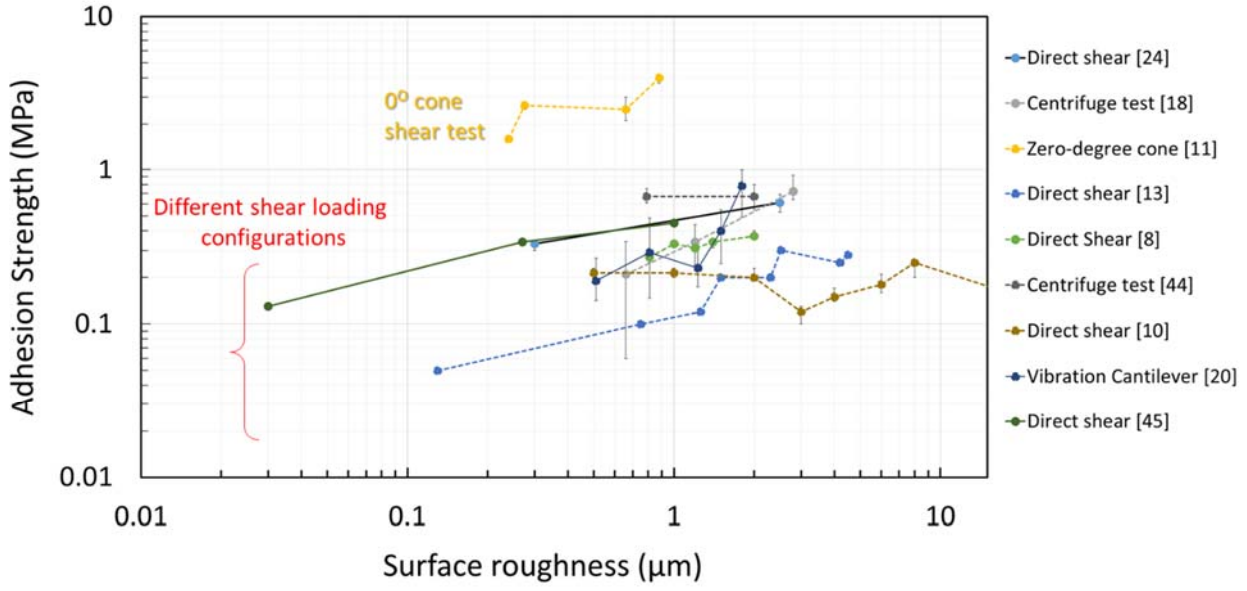

Fig. 1 Summary of reported ice adhesion strength for an ice/aluminum interface using different experimental loading configuration. A full order of magnitude difference can be observed between 0° cone angle shear test and other testing configuration.

The observed discrepancy of shear strength between the test methods has not been fully understood yet. Moreover, the dependency on the mode of interface loading is also critical, as tensile and shear strengths of the interface were reported to be different [12]. Moreover, the utilization of elastomeric icephobic surfaces has exposed the role of interfacial cavitation to reduce the shear strength of ice adhesion [27-29]. Cavitation is a primarily tension driven phenomenon [30]; thus, it is important to quantify the difference if any, between shear and tensile adhesion of the ice-solid interface. This paper embraces a fracture mechanics approach to delineate the difference between direct-shear and push-out tests. It also highlights the response of near mode-I or a tensile fracture of the interface utilizing a specially designed single cantilever beam [31, 32] with those derived under mode-II shear fracture. Summary of testing configurations, finite element calibration of cohesive parameters for each of the failure modes, and summary of the critical results are given.

III. Experimental Framework

A generalized testing frame is designed and built inside an environmental chamber, as highlighted in Fig. 2. The loading cross-head is a pneumatically controlled cylinder driven by dry nitrogen gas through a three-way valve. The force and displacement were recorded using a load cell (FUTEK-100Ib) and linear variable differential transducer (Lucas Schaevitz), respectively. These sensors were calibrated at the same testing temperature range of the testing protocol. A set of needle valves were employed to set the flow rate and thereby control the loading rate between 2.5-7.5 N/s. Different sample holders can be attached to the testing frame, as highlighted in Fig. 2(b) for a single cantilever beam (SCB) to test the ice-substrate interface at near mode-I tensile fracture, Fig. 2(c) for a direct shear testing configuration to test the ice-substrate interface at near mode-II loading, and Fig. 2(d) for push-out shear testing configuration with also a near mode-II fracture loading.

Al 6061-T6 substrates were utilized in all tests. The substrate surface was ground using silicon carbide grinding papers with different grit sizes (80-2000 grits), providing more than an order of magnitude change in the root mean square surface roughness, RMS=0.05-4.3µm (over a 1.1x1.1mm window). The surface roughness was measured by a non-contact surface profilometer (Zygo Newview 6200). A two-step surface cleaning was applied to each surface with acetone and methanol and then was air-dried. Each surface was tested only once after preparation and then reground for subsequent testing to reduce the interference of native oxide formation on the surface. De-ionized water was utilized to cast all ice specimens. The ice samples were formed and kept inside an environmentally controlled chamber for 24 hours before testing. All reported samples here in this work were tested at -17.5° C. The samples' geometries and the testing boundary condition for each loading configurations are shown in Fig. 2(b-d).

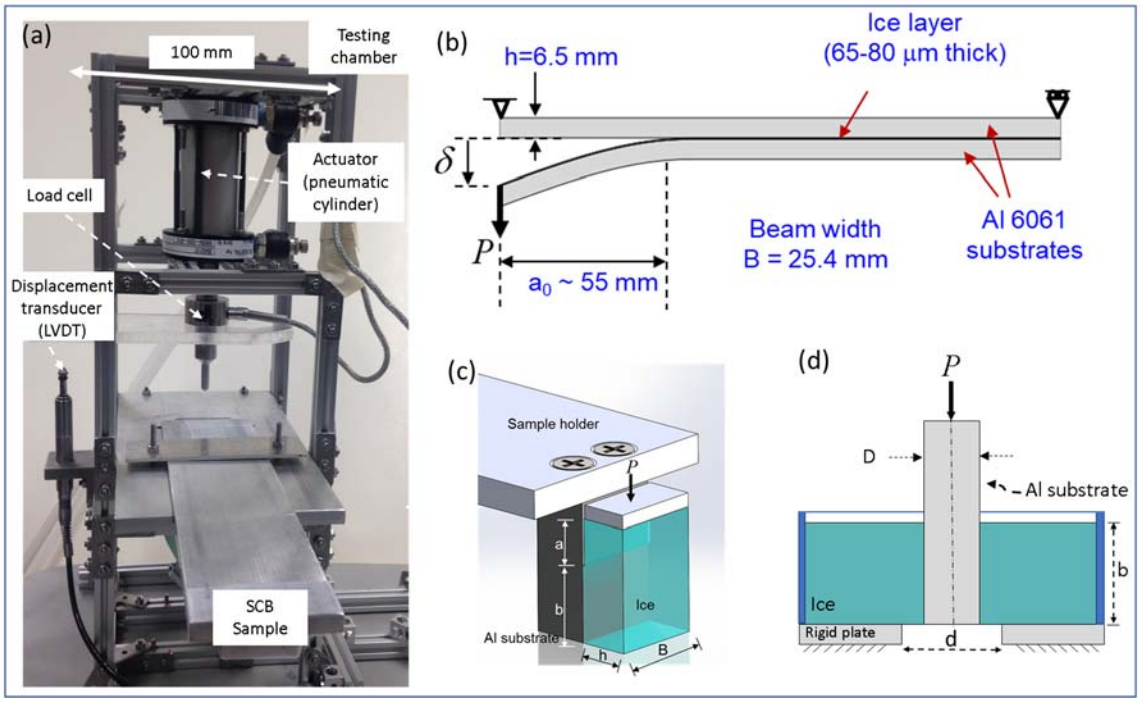

Fig. 2 (a) Developed universal testing setup. (b) Single cantilever beam testing configuration. (c) Direct shear-testing configuration. (d) Push-out testing configuration.

A. Single Cantilever Beam (SCB) Configuration

A modified SCB sample is adapted here for ease of loading, derived from the standard double cantilever beam [33], typically used to examine the interfacial adhesion of laminates. A thin ice layer is formed between two aluminum beams. One of the beams (2" wide and 7.5" long) is fixed to the frame, while the other deformable beam (1" wide and 8" long) is subjected to the loading until failure (Fig 2(b)). In this configuration, a predefined crack of a = 55 mm length is created by coating one of the beams with a hydrophobic coating to prevent ice formation. Droplets of de-ionized water are applied between the two beams, before being assembled to form the contained interfacial ice layer of 65-80 μm thickness (for more details on this configuration see Ref. [31-32]). The near mode-I interfacial fracture energy is calculated from the measured $P-\delta$ curve, using the modified beam theory [34],

$$\Gamma_I \equiv G\big|_{a=a_c} = \frac{3P\delta}{2B\,a}. \tag{1}$$

P is the applied load, δ is the vertical beam displacement, B is the ice width, and a is the instantaneous crack length, as indicated in Fig. 2(b). In a typical interface fracture with large scale bridging [33], the instantaneous crack length a should be independently measured. However, for the current ice/aluminum interface, with limited process zone ahead of the interfacial crack tip, a can be calculated from the beam elastic deflection, δ

$$a = \left(\frac{3E_{Al}\,I}{P/\delta}\right)^{1/3}. \tag{2}$$

E_{Al} is the beam young's modulus, and I is the beam section moment of area. It should be noted that before the start of crack propagation, the beam stiffness P/δ is almost constant, which is being utilized to identify the initiation of crack propagation. This approximation was verified by finite element analysis of the testing configuration [31-32].

B. Direct Shear Configuration

The direct shear samples were produced by forming an ice block on an aluminum substrate within a soft enclosure. After freezing, the mold is removed, and the ice dimensions were measured prior to testing. Ice blocks were loaded under shear till failure, as depicted in Fig. 2(c). The range of tested surface roughness was RMS=0.04-4.1 μm. Different ice block lengths of b= 5-57 mm were examined in this study. From the applied load and the ice contact area, the interfacial ice adhesion strength τ_c is calculated through

$$\tau_c \equiv \frac{P}{A} = \frac{P}{b\,B}. \tag{3}$$

The near mode-II fracture energy Γ_{II} is calculated using J-integral [35],

$$\Gamma_{II} \equiv J = Z\frac{(P/B)^2}{2\,E_{ice}\,h}. \tag{4}$$

Where P is the load, $A = b\,B$ is the area to be sheared of uncracked ligament and B is the ice width, E_{ice} is Young's modulus of ice, h is the ice layer thickness. Noteworthy is that the mode-II toughness of the direct shear test is independent of the crack length. This equation was originally derived for a thin film on a rigid substrate system; however, the ice layer thickness is considered to be thick in the current test configuration. Therefore, a scaling factor Z was included in the calculation and estimated numerically to be $Z = 1.32$ from a set of finite element simulations for the range of test geometries. The Young's modulus of ice, E_{ice} is estimated from the specimen stiffness (the initial slope of the loading curve before crack propagation) and was found to be approximately 5 *GPa* for the different loading configuration examined and for the static ice under laboratory conditions. It should be noted that different values have been estimated for the ice modulus and were found to depend on the ice formation conditions (static vs. impact), the environmental temperature, and the aging process. All these parameters would change the underlying microstructure, grain size, and defect content within the ice. The average reported values were in the range 2-9 *GPa* [24, 35-37].

C. Zero Degree Cone Angle Push-out Test

The push-out sample was made by forming the ice around an aluminum rod, centered on a lubricated substrate, and contained within a plastic retainer cylinder to form the ice cylinder, as depicted on Fig. 2 (d). The aluminum rod was ground by 600 grit size sandpaper providing RMS surface roughness about 0.4 μm (see Ref. [22] for more details

about sample preparation). The test is conducted by progressively pushing the aluminum rod until it is completely pushed- out of the ice sheet (full failure). From the applied load and the ice contact area, the average interfacial ice adhesion strength τ_c is calculated by assuming a uniform shear distribution at the interface through

$$\tau_c \equiv \frac{P}{A} = \frac{P}{\pi D\, b}. \tag{5}$$

For the push-out shear test configuration, a shear-lag model was used to analytically estimate the near mode-II interfacial toughness from the experimental measurements. The analysis employs force balance in the vertical axis between the axial stress in the rod and the shear stress at the interface [38, 39]. Based on the shear-lag model, the interface stiffness is given as,

$$K_{\text{interface}} \equiv \left(\frac{P}{\delta}\right)_{ave} = \frac{\pi\, E_{Al}\, D^2}{4\,\lambda} \tanh\left(\frac{b}{\lambda}\right). \tag{6}$$

Where $\left(P/\delta\right)_{ave}$ is the average of the measured interface stiffness, obtained after subtraction of the machine compliance and the bulk ice compliance (calibrated from FEM with perfect adhesion interface) from the experimentally measured force-displacement data in push-out test. E_{Al} is Young's modulus of the aluminum rod, D is the rod diameter, b is the ice adhesion length (cylinder height), and λ is a characteristic length scale; $\lambda = \sqrt{E_{ice} D / 4k_s}$ depending on the initial slope of the traction-separation curve k_s (which will be also used in the FEA of the push-out test). Eq. (6) is then solved iteratively for k_s. From the experimentally measured τ_c and k_s, the mode-II fracture toughness can be derived by integrating the curve as,

$$\Gamma_{II} = \frac{\tau_c^2}{2k_s}. \tag{7}$$

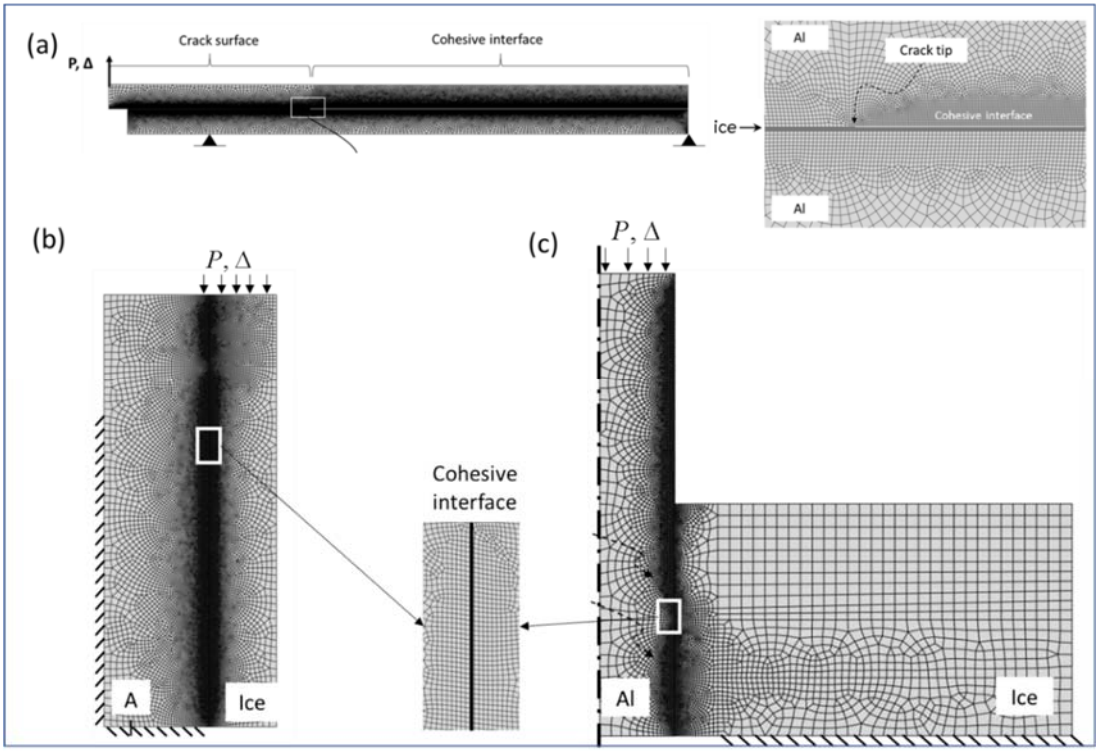

Fig. 3 Finite element models for (a) SCB(plain strain) , (b) direct shear (plane strain) and (d) push-out shear (axisymmetric) testing geometries.

IV. Finite Element Simulation

In numerical analysis, finite element (FE) simulations incorporating cohesive surface approach were performed using Abaqus/CAE 2016. The SCB and direct shear samples were modeled using 4-node bilinear plane strain elements (CPE4R), while the push-out test sample was modeled using 4-node bilinear axisymmetric quadrilateral elements (CAX4R). The utilized FE geometric models with the employed mesh and boundary conditions are shown in Fig. 3. The geometry and boundary conditions used in the numerical simulations were selected to match the experimental counterparts. Both ice and aluminum beams were modeled as isotropic elastic materials with mechanical properties $E_{ice} = 5\ GPa,\ \nu_{ice} = 0.3$ and $E_{Al} = 70\ GPa,\ \nu_{Al} = 0.33$ for ice and aluminum, respectively. The adhesion between the ice and aluminum substrates was simulated using a cohesive surface with a bilinear traction-separation law, and the crack surfaces were taken to be frictionless. The global mesh size was selected to be 0.5 mm, while the mesh is refined along the cohesive zone, as shown in Fig. 3. The refined mesh size of 0.05 mm was used along the cohesive zone. The refined mesh size was chosen to be sufficiently smaller than the cohesive zone length [40]. A convergence study was also performed to verify the mesh-independency of the model.

Figure 4 shows the opening and shear stress fields in the vicinity of the crack tip. The phase angle of fracture mode-mixity was assessed by linear elastic fracture mechanics-based finite element analysis for the examined test geometries. The phase angle was calculated by evaluating the ratio of the shear stress and opening stress values at a distance in front of a stationary crack tip with tied boundary, using the definition $\psi = \tan^{-1}\left(\tau_{12}/\sigma_{11}\right)$. The corresponding phase angles were obtained to be $\psi = -31^{o}$ for SCB specimen, $\psi = 85^{o}$ for direct shear specimen and $\psi = -82^{o}$ for the SCB for push-out shear fracture tests, respectively. The mode-I and mode-II cohesive traction-separation curves contain three independent fracture parameters: the initial slope of the curves (k_n, k_s) the critical cohesive stresses ($\hat{\sigma}, \hat{\tau}$) and cohesive fracture energy (Γ_I, Γ_{II}). k_n was selected to be $k_n = 100\ MPa/\mu m$ [46-47], which is large enough to eliminate numerical divergence in SCB simulations. k_s was obtained to be $k_s = 0.35\ MPa/\mu m$ by iterative solution of Eq. (6) using the experimental data from the push-out shear tests. The remaining two fracture parameters ($\hat{\sigma}, \hat{\tau}$) and (Γ_I, Γ_{II}) were determined by matching the experimentally measured force-displacement curves [22]. A parametric study was carried out to extract the cohesive fracture parameters, listed in Table 1. First, the experimentally derived mode-I and mode-II toughness values were used as the initial values of (Γ_I, Γ_{II}). Then, ($\hat{\sigma}, \hat{\tau}$) were varied in a particular range to match the maximum force of the load-displacement curves of the experimentally measured values for each testing configuration. Each mode was calibrated separately without enforcing a mixed mode constitutive relation for fracture energy.

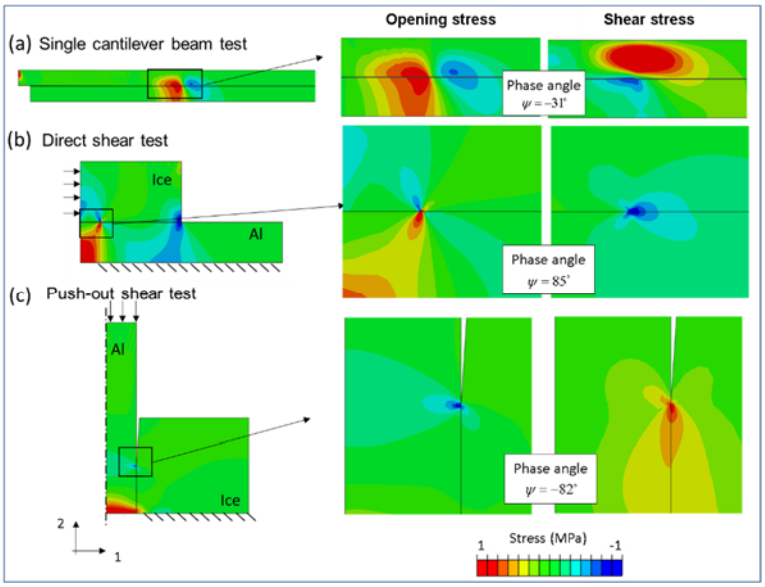

Fig. 4 FEM results for opening and shear stress fields near the crack tip for all examined configurations.

V. Results

The general trend of the measured interfacial fracture energy is summarized on Fig. 5 for the near mode-I tensile SCB and near Mode-II direct shear configurations (b=*13 mm* and B= *20 mm*) as a function of surface RMS roughness. All measurements are the average of at least 5-samples with one standard deviation marked on each data set. All measurements were carried out at -17.5 ºC. For the tested range of surface roughness, the interfacial fracture energy for both configurations was found to have approximately the same average level of the interfacial fracture energy of about $0.5-0.6\ J/m^2$. It is also worth noting that the direct shear results revealed much smaller variability compared to those form repeat tensile SCB tests. This might be attributed to a wide range of statistical entrapment of interfacial defects between the two beams of the SCB configuration. However, there are two key observations that could be highlighted here for the range of the examined roughness, which spans two orders of magnitudes. *First*, it is apparent that the work of adhesion is insensitive to the applied mode of loading, of whether being tensile or shear fracture. *Second*, the interfacial adhesion energy is almost independent of the surface roughness. Any subtle variation is almost within the experimental variability for the whole experimental trend. This data is in a direct contrast with the observed trends, summarized on Fig.1 wherein there is both large scatter and perceived weak dependence of ice-solid adhesion strength with roughness. This contrast highlights the need of a well-controlled fracture mechanics based experiment, to avert the influence of different geometrical artifacts. Moreover, a similar trend and levels for the interfacial work of adhesion were also found in a shaft driven blister test [48], which has the same range of phase angle, $\psi=-30^o$ to -34^o similar to SCB configuration.

The observed trend of loading mode insensitivity and roughness insensitive effect on the interfacial work of adhesion are corroborating with each other. Typically, rough interfaces would result in increased effective interfacial fracture toughness due to asperity locking [26]. However, this typically occurs when an adhesive-failure dominates the interfacial adhesion failure mechanism. In the current work, both the SCB configuration and the direct shear configuration showed a consistent cohesive interface failure. Though, for the SCB, the interfacial crack was driven away from the interface due to mode mixity, wondering between the interfaces of the two loading beams, but remains within the ice-phase only [31]. A limited set of SCB samples with $RMS<0.3\ \mu m$ exhibited a failure mode transitioned to adhesive failure with reduced work of adhesion to the range $\sim 0.2\ J/m^2$. Thus it could be concluded that when the same failure mode is prevailed, no loading mode dependency, or roughness dependency may be anticipated. However, this observation/conclusion should be further examined with polymer-based interfaces that might stimulate stress localization at the interface with inhomogeneous stress distribution at the submicron level [29].

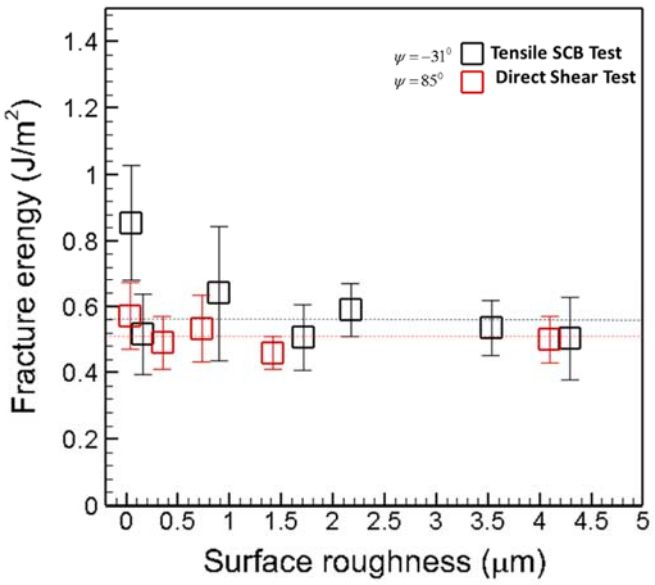

Fig. 5 Summary for the experimental measurements for the interfacial fracture energy as a function of the surface RMS roughness at *-17ºC*. SCB samples are for *a=55* mm crack, and direct shear samples have *b=13mm* ligament and *B=20mm* width.

A set of direct shear samples ranging with *b=5-57 mm* and push-out samples with b= 5-8 mm, were tested. The examined set highlights the role of testing configuration, confinements as well as the sheared length, *b* on the interfacial fracture parameters for both configurations. Figure 6 summarizes the critical adhesion force for either nucleation, or full unstable ice shear-off, normalized by the ice width, *B*, with respect to the sheared length, *b*. The measurements show a linear correlation between the normalized force P/B and *b*, wherein the initial slope of the best-fit line represents the interfacial adhesion strength, τ_c. The measurements shows that push-out test ($\tau_c = 2210\ kPa$) is about eight-times larger than the direct shear results ($\tau_c = 270\ kPa$). This is in agreement with reported data for the zero-degree cone test [11] in contrast to other loading configures, as shown in Fig. 1. Such effect is a direct outcome from the residual stress generated during the freezing process, arising from the axisymmetric constrains on the volumetric expansion within the plane of the ice. Such effect would be relaxed in the out of plane direction for a planer configuration. The calibrated FEA prediction is also imposed on the experimental trend. It should be also noted that for longer ice samples, the failure mode changes from shear strength dominated to crack-nucleation and propagation dominated failure. The transition between the modes sets the critical ice length scale, b_{cr} wherein a stable crack propagation could be observed for larger samples [25].

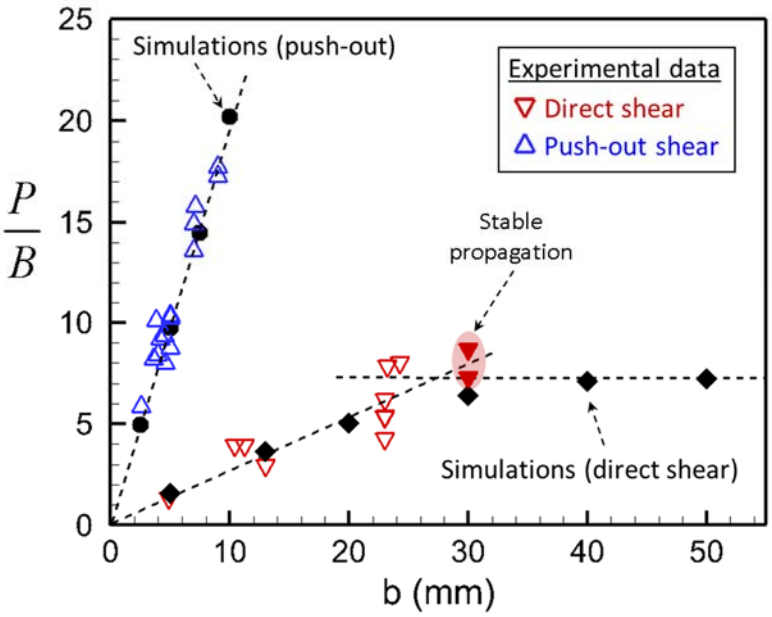

Fig. 6 Summary of the experimental and numerical results for the interfacial normalized decohesion force (by the sample width) vs. the shear ice length for both the direct shear and push-out shear tests. The initial slope of the curve is the interfacial shear strength of the ice-solid interface.

The utilized traction separation laws, based on fitting the experimental results, are summarized in Fig. 7. There are several subtle details in these simulations and fitting to the experimental results, which are critical for understanding the difference between the tensile and shear behavior of the ice/solid interface. First, the experimental measurements showed that the tensile and shear mode loading have the same interfacial fracture energy. However, each mode have very different traction-separation relation with different cohesive strength and critical cohesion length. This difference arises from the difference of the interface stiffness under the normal and shear-loading mode, as summarized in Table-1. This also implies that the bridging length scale in shear is much bigger (at least three times as big) compared to tensile fracture. This relative scale might play a greater role in the design of icephobic surfaces with stress concentration features that stimulate tensile cavitation [29]. It would set the critical size feature needed to reduce interfacial adhesion. Second, the push-out test has an order of magnitude increase in the interfacial adhesion, arising from constrained volumetric expansion, which induces compressive residual stresses. These compressive stresses on the interface would greatly increase both the interface stiffness and the critical decohesion shear displacement. Again, matching the observed experimental trends resulted in these characteristics of the cohesive surfaces for each case.

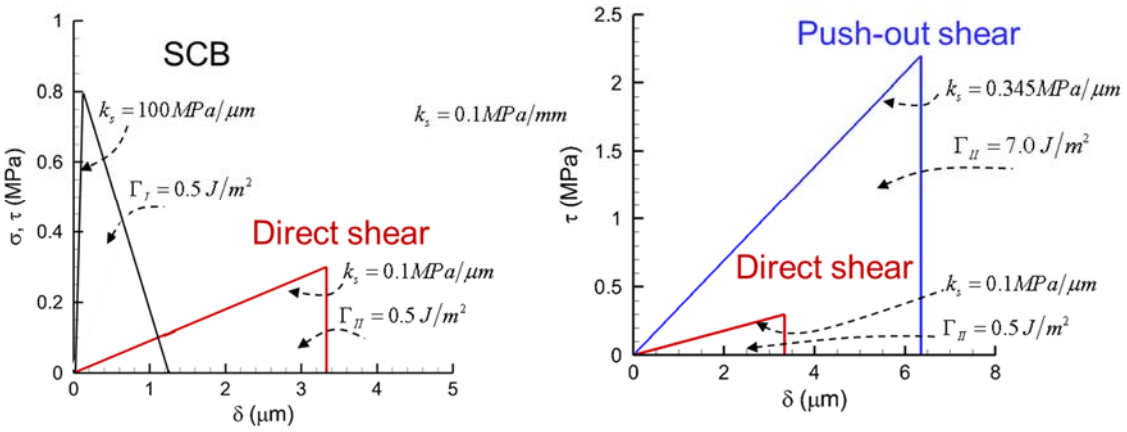

Fig. 7 The experimentally guided and numerically fitted bilinear traction-separation correlations for (a) normal and shear cohesive relations, and (b) shear cohesive relationship for different shear configurations.

Figure 8 summarizes the fitting of the FEA prediction with the calibrated cohesive surfaces to the experimentally measured different configurations. The FEA simulation well replicates the experimentally measured trends, especially with the limited crack propagation observed in the SCB configuration and the unstable crack propagation for the short sheared samples for direct shear test and push-out tests. The dimensions of both of these configurations were selected to be in the strength dominated regime, wherein an unstable failure would be prevalent.

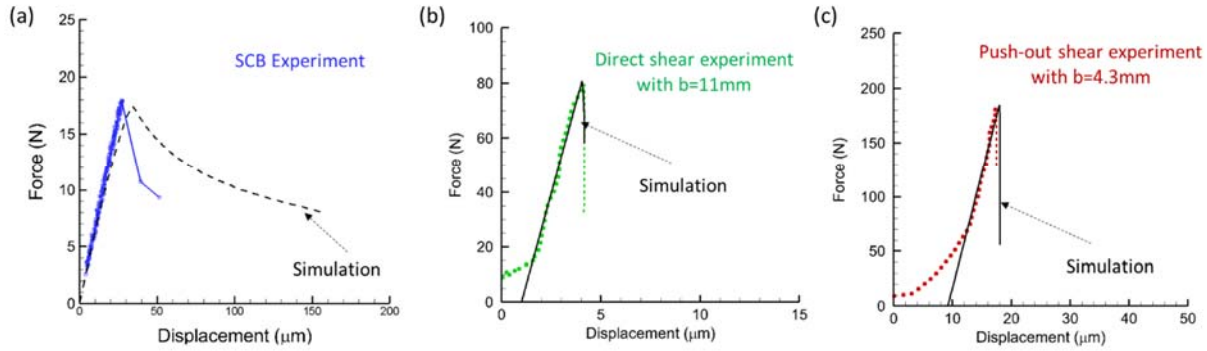

Fig. 8 Comparison between the experimental measured and FEA simulated force-displacement curves obtained for the different configurations. (a) Single cantilever beam test. (b) Direct shear test. (c) Push-out test.

Table 1 Analytical and numerical interfacial fracture parameters for Direct shear and push-out tests

	Experimentally Fitted			Numerical		
	k_s (MPa/μm)	$\hat{\sigma}$ or $\hat{\tau}$ (MPa)	Γ_I or Γ_{II} (J/m^2)	k_s (MPa/μm)	$\hat{\sigma}$ or $\hat{\tau}$ (MPa)	Γ_I or Γ_{II} (J/m^2)
Tensile (Mode-I)	-	-	0.56	100	0.8	0.5
Direct shear- (Mode-II)	-	0.27	0.48	0.100	0.35	0.5
Push-out (Mode-II)	0.345	2.21	7.05	0.345	2.20	6.98

VI. Conclusions

A fracture mechanics based approach is utilized to understand the role of testing configuration geometry on the adhesion of ice-solid interface. Three different geometric configurations were studied, including a near mode-I single cantilever beam configuration, and a near mode-II and a direct shear and push-out configurations. The experimental results showed that the effective work of adhesion is both insensitive to the mode of loading and the roughness of the solid interface for the range of performed experimental measurements and for the observed cohesive interfacial failure. The role of surface roughness induced asperity locking was completely absent for the observed cohesive interfacial failure. Moreover, the experimental results showed almost an order of magnitude increase in both the work of adhesion and the critical shear strength of the interface for the push-out test, compared to the direct shear test. Such significant enhancement arises of the axisymmetric geometric constraints on the lateral expansion within the plan of the ice, leading to increase compressive stresses on the interface. The FEA cohesive surface analysis has highlighted the relative scale of the critical cohesive displacement at the interface under normal and shear loading, which could be utilized in the design of icephobic surface.

Acknowledgments

This work was supported by NASA grant number NNX16AN21A, with Mr. Richard Kreeger as the technical officer, and by Iowa State University through the T.W. Wilson Professorship.

References

[1] Andersson, A.K., and Chapman, L., "The impact of climate change on winter road maintenance and traffic accidents in West Midlands, UK," Accid. Anal. Prev., Vol. 43, 2011, pp. 284–289. doi.org/10.1016/j.aap.2010.08.025

[2] Gent, R.W., Dart, N.P., and Cansdale, J. T., "Aircraft icing," Philos. Trans. R. Soc. London, Vol. 358, 2000, pp. 2873–2911. doi.org/10.1098/rsta.2000.0689

[3] Lynch, F.T, and Khodadoust, A., "Effects of ice accretions on aircraft aerodynamics," Progress in Aerospace Sciences, Vol. 37, No. 8, 2001, pp.669-767. doi.org/10.1016/S0376-0421(01)00018-5

[4] Berkman, P.A., Fiske, G., Røyset, JA., Brigham, L.W., Lorenzini, D., "Next-Generation Arctic Marine Shipping Assessments," Governing Arctic Seas: Regional Lessons from the Bering Strait and Barents Sea. Informed Decisionmaking for Sustainability, edited by O. Young, P. Berkman, A. Vylegzhanin, Springer, Cham, 2020, pp. 241-268. doi.org/10.1007/978-3-030-25674-6_11

[5] Savadjiev, K., and Farzaneh, M., "Modeling of icing and ice shedding on overhead power lines based on statistical analysis of meteorological data" IEEE Trans. On Power Delivery, Vol. 19, No. 2, 2004, pp. 715-721. https://ieeexplore.ieee.org/stamp/stamp.jsp?tp=&arnumber=1278431

[6] Fortin, G., and Perron, J., "Wind turbine icing and de-icing," 47th AIAA Aerospace Sciences Meeting Including The New Horizons Forum and Aerospace Exposition, AIAA 2009-274, Orlando, Florida, 2009. doi/pdf/10.2514/6.2009-274

[7] Bragg, M., Gregorek, G., Lee J., "Airfoil aerodynamics in icing conditions, " J Aircr., 23, 1986, 76–81.

[8] Chu, MC, Scavuzzo, RJ. "Adhesive shear strength of impact ice," AIAA J, 1991; 29:1921–6.

[9] Rønneberg, S., Zhuo, Y., Laforte, C., He, J., Zhang Z., "Interlaboratory study of ice adhesion using different techniques," Coatings, 9(10), 2019, 678, DOI, 10.3390/coatings9100678

[10] Dong, W., Ding, J., Zhou, Z.X., "Experimental Study on the Ice Freezing Adhesive Characteristics of Metal Surfaces," Journal of Aircraft, 2014 51:3, 719-726.

[11] Susoff, M., Siegmann, K., Pfa_enroth, C., Hirayama, M., "Evaluation of icephobic coatings—Screening of different coatings and influence of roughness," Applied Surface Science, 282, 2013, 870–879.

[12] Laforte, C, Laforte, JL., "Tensile, torsional and bending strain at the adhesive rupture of an iced substrate," Proceedings of the ASME 28th international conference on ocean, offshore and arctic engineering, 2009, p. 79–86. https://doi.org/10.1115/OMAE2009-79458.

[13] Druez, J., Phan, C.L., Laforte, J.L., Nguyen, D.D., "The adhesion of glaze and rime on aluminum electrical conductors," Trans. Can. Soc. Mech. Eng., 5 (4), 1979, 215–220.

[14] Jellinek, H.H.G., "Adhesive properties of ice", Journal of Colloid Science, Vol. 14., 1959, pp. 268-280.

[15] Pervier, M.L.A., et al., "A new test apparatus to measure the adhesive shear strength of impact ice on titanium 6Al-4V alloy," Engineering Fracture Mechanics,. Vol. 214, 2019, pp. 212-222. https://doi.org/10.1016/j.engfracmech.2019.01.039

[16] Raraty, L. E., Tabor, D., "The adhesion and strength properties of ice," Proceedings of the Royal Society of London. Series A, Mathematical and Physical, Vo. 245, No. 1241, 1958,PP.184-201.

[17] Stallabrass, J.R., and Price, R.D., "On the adhesion of ice to various materials," National Research Council Canada,1962.

[18] Soltis, J., Palacios, J., Wolfe, D. and Eden, T., “Evaluation of ice adhesion strength on erosion resistant materials,” In 54th AIAA/ASME/ASCE/AHS/ASC Structures, Structural Dynamics, and Materials Conference, 2013, p. 1509.
[19] Mulherin, N.D., Richter-Menge, J.A., Tantillo, T.J., Gould, L.D., Durell, G.D. and Elder, B.C., “Laboratory test for measurement of adhesion strength of spray ice to coated flat plates,” (No. CRREL-90-2), 1990..
[20] Hassan, M.F., Lee, H.P., and Lim, S.P., “The variation of ice adhesion strength with substrate surface roughness, “Measurement Science and Technology, 21(7), 2010, p.075701.
[21] Meuler, A J, Smith, J D, Varanasi, K K, Mabry, J M, McKinley, G H, and Cohen, R E, “Relationships between Water Wettability and Ice Adhesion,” Appl. Mater. Interfaces, 2 (11), 2010, pp 3100–3110.
[22] Yavas, D., Bastawros, A., Dawood, B., and Giuffre, C., "Characterization of Mode-II Interfacial Fracture Toughness of Ice/Metal Interfaces," SAE Technical Paper, 2019-01-1947, 2019, https://doi.org/10.4271/2019-01-1947.
[23] Haehnel,R., Mulherin,N., “The bond strength of an ice–solid interface loaded in shear,” in: H.T. Shen (Ed.), Ice in Surface Waters. Proceedings of the 14th International Symposium on Ice, Kinokuniya Company Ltd, 1998.
[24] Reich, A., Scavuzzo, R., and Chu, M., “Survey of Mechanical Properties of Impact Ice,” AIAA Paper 1994-712, Jan. 1994.
[25] Golovin, K., Dhyani, A., Thouless, M. D., Tuteja, A. "Low–interfacial toughness materials for effective large-scale de-icing", Science, 364, 2019, pp. 371- 375.
[26] Evans A. G., Hutchinson J. W. “Effects of non-planarity on the mixed mode fracture resistance of bimaterial interfaces.” Acta Metallurgica, Vol. 37, No. 3, 1989, pp. 909-916. doi.org/10.1016/0001-6160(89)90017-5
[27] Golovin, K., Kobaku, S.P.R., Lee, D.H., Diloreto, E.T., Mabry, J.M., Tuteja, A., “Designing durable icephobic surfaces,” Science advances, Vol. 2, No. 11, 2016, e1501496. DOI: 10.1126/sciadv.1501496
[28] Beemer, D.L., Wang, W., Kota, A.K., “Durable gels with ultra-low adhesion to ice,” J. Mater. Chem. A. 4, 2016, pp. 18253-18258. doi.org/10.1039/c6ta07262c
[29] Irajizad, P., Al-Bayati, A., Eslami, B., Shafquat, T., Nazari, M., Jafari, P., Kashyap, V., Masoudi, A., Araya, D., Ghasemi, H., “Stress-localized durable icephobic surfaces,” Mater. Horizons 6, 2019, pp. 758–766. doi.org/10.1039/c8mh01291a
[30] X. Sun, L. Yu, M. Rentschler, H. Wu, R. Long, PT US CR, “Delamination of a rigid punch from an elastic substrate under normal and shear forces,” J. Mech. Phys. Solids., Vol 122, 2019, pp. 141-160. doi.org/10.1016/j.jmps.2018.09.009
[31] Dawood, B., Yavas, D., Giuffre, C., and Bastawros, A., "Utilization of Single Cantilever Beam Test for Characterization of Ice Adhesion," SAE Technical Paper, 2019,-01-1949. https://doi.org/10.4271/2019-01-1949.
[32] Dawood, B., Giuffre, C., and Bastawros, A., “Fracture Mechanics Based Approach for Ice Adhesion Characterization,” in 2018 Atmospheric and Space Environments Conference, 2018, 10.2514/6.2018-3343. https://doi.org/10.2514/6.2018-3343
[33] ASTM-D5528-13, “Standard Test Method for Mode-I Interlaminar Fracture Toughness of Unidirectional Fiber-Reinforced Polymer Matrix 357 Composites,” ASTM International, West Conshohocken, PA, Standard No. 358, ASTM, 2013.
[34] William, JG. “The fracture mechanics of delamination tests,” Journal of Strain Analysis, 24(4), 1989, 207-214.
[35] Suo, Z., and Hutchinson, J.W., “Interface crack between two elastic layers,” International Journal of Fracture, 43(1), 1990, pp.1-18.
[36] Work, A., Lian, Y., “A critical review of the measurement of ice adhesion to solid substrates,” Prog. Aerosp. Sci., 98, 2018, pp. 1-26, 10.1016/j.paerosci.2018.03.001, 2018.
[37] Traetteberg, A., Gold, L. W., and Frederking, R. M. W., “The strain rate and temperature dependence of Young’s modulus of ice.” Proc., IAHR 3rd Int. Symp. on Ice Problems, International Association for Hydro-Environment Engineering and Research (IAHR), New York, 1975, 479–486.
[38] Takaku, A., and Arridge, R.G.C., “The effect of interfacial radial and shear stress on fiber pull-out in composite materials,” Journal of Physics D: Applied Physics, 6(17), 1973, p.2038.
[39] Wu, C., Huang, R., and Liechti, K.M., “Characterizing Interfacial Sliding of Through-Silicon-Via by Nano-Indentation,” IEEE Transactions on Device and Materials Reliability, 17(2), 2017, pp.355-363.
[40] Turon, A, Davila, CG, Camanho, PP, Costa, J., “An engineering solution for mesh size effects in the simulation of delamination using cohesive zone models,” Engineering fracture mechanics, 74(10), 2007 p.1665-1682.
[41] Yavas, D, Shang X, Bastawros, AF, “Mode-I fracture toughness and surface morphology evolution for contaminated adhesively bonded composite structures,” Composite Structures, 2018 Nov 1;203:513-22.
[42] Zou, M., Beckford, S., Wei, R., Ellis C., Hatton, G., Miller, “M.A., “ Effects of surface roughness and energy on ice adhesion strength,” Applied surface science, 254, 2011, pp.3786:3792, USA.
[43] Wang, C., Zhang,W., Siva, A., Tiea, D.;Wynne, K.J. “Laboratory test for ice adhesion strength using commercial instrumentation,” Langmuir, 2014, 30, 540–547.
[44] Guerin, F., Laforte, C., Farinas, M. I., Perron, J., “Analytical model based on experimental data of centrifuge ice adhesion tests with different substrates,” Cold Reg. Sci. Technol., 2016, 121, 93–99.

[45] Beeram, P.S.R., Waldman, R.M., Hu, H., “Measurements of Ice Adhesion over Ice Mitigation Coatings Pertinent to Aircraft Icing and Anti-/De-Icing,” in: 9th AIAA Atmos. Sp. Environ. Conf., 2017. doi:10.2514/6.2017-3928.
[46] Yavas, D., Shang, X., Hong, W., and Bastawros, A.F., “Utilization of nanoindentation to examine bond line integrity in adhesively bonded composite structures,” Int. J. Fracture, Vol. 204, 2017, pp. 101-112. doi.org/10.1007/s10704-016-0165-z
[47] Yavas, D., Shang, X., and Bastawros, A.F., “Mode-I fracture toughness and surface morphology evolution for contaminated adhesively bonded composite structures,” Composite Structures, Vol 203, 2018, pp.513-522. doi.org/10.1016/j.compstruct.2018.07.014
[48] Giuffre, C., Dawood, B., Yavas, D., and Bastawros, A., “Numerical and experimental investigation of ice adhesion using the blister test,” SAE Technical Paper, 2019,-01-1948. doi.org/10.4271/2019-01-1948